PERGAMON

Computers and Structures 72 (1999) 459–480

Computers & Structures

www.elsevier.com/locate/compstruc

Nonlinear mechanical behaviour and analysis of wood and fibre materials

Stefan Holmberg[a], Kent Persson[a], Hans Petersson[b,*]

[a]*Division of Structural Mechanics, Lund University, Lund, Sweden*
[b]*Department of Structural Mechanics, Chalmers University of Technology, Göteborg, Sweden*

Received 16 October 1998

Abstract

The mechanical behaviour of wood was studied from a micro up to a macro level. Wood is a cellular material possessing a high degree of anisotropy. Like other cellular solids, it often exhibits a highly nonlinear stress–strain behaviour. In the present study the mechanical properties of the cellular structure of wood are characterized and modelled, the irregular cell shape, the anisotropic layered structure of the cell walls and the periodic variations in density being taken into account. The continuum properties were derived by use of a homogenization procedure and the finite element method. Stiffness and shrinkage properties determined by this procedure are presented and are compared with measured data. The constitutive properties thus determined at various structural levels can be used in numerical simulations of the behaviour of wood in different industrially related areas. One such area is that of the refining process in mechanical pulp manufacture. Simulations of the deformation and fracturing of wood specimens loaded under conditions similar to those found in the refining process are presented. The numerical and experimental results obtained are compared.

Keywords: Cellular materials; Wood; Mechanical behaviour; Microstructure; Homogenization; Finite element method; Constitutive models; Defibration

1. Introduction

Although wood is widely used as an engineering material, there is still a substantial lack of understanding of its material behaviour, from a micro to macro level. There is thus a definite need for an improved understanding of wood at a micro level and of integrating this with knowledge of its behaviour on different scales extending up to that of structural performance. Obtaining a more precise material description of wood than is available today could enable the vision of wood as a well-defined engineering material for industrial products. Wood and timber products should have measurable properties that are clearly defined with well documented performance. The application to wood science of modern material science and of structural mechanical methods, particularly at the micro level, provides the impetus for this development. This can be seen in Fig. 1, which shows the chain extending from a micro to a macro level together with the respective levels of modelling. At the micro level, such important factors as fibre shape, cell wall thickness and microfibril angle are considered. The properties of clear wood can be described in terms of these factors, combined with growth characteristics. Starting with the clear wood properties and taking such log imperfections as knots, spiral grain and the like into account, one can

* Corresponding author.

0045-7949/99/$ - see front matter
PII: S0045-7949(98)00331-9

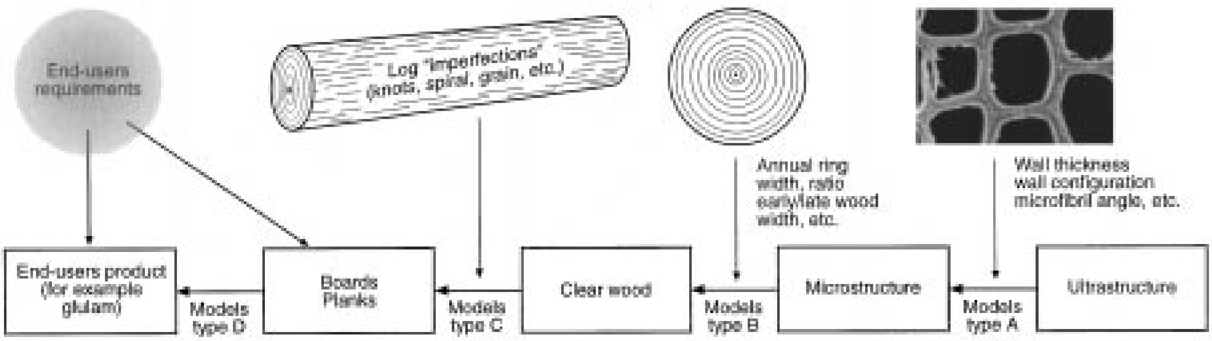

Fig. 1. Modelling chain for wood extending from ultra-structure to end-user products.

define the behaviour of sawn and dried timber rather precisely by use of proper models. Such a defining of properties can be attained by use of computer simulations combined with modern measuring techniques. At the highest level, models for various engineering products can be used to verify end-user requirements being fulfilled.

Before the vision of wood as a well-defined engineering material can become a reality, much research is yet to be carried out. There are, however, several ongoing projects in Sweden which, with reference to Fig. 1, aim at finding proper models of type A, which deals with microstructure, up to macromodels of types C and D. These macromodels are used to check on how well various end-user requirements are fulfilled. The most important end-user requirements for timber and wood products tend to be the following:

- that structural elements should have enough load-bearing capacity (strength), as illustrated by the curved glulam beam shown in Fig. 2a [1,2];
- that timber should be sufficiently stable in shape and dimension and not be distorted too much by variations in moisture, illustrated by the distorted beam shown in Fig. 2b [3–5].

In the both cases shown in Fig. 2, the behaviour of wood is strongly dependent upon its orthotropic material properties and their distribution in space. To obtain realistic results in analysing the structural behaviour of wood, selection of a proper constitutive model and choice of the data to use for the material parameters in the model are crucial. The material data for wood is strongly influenced by the type of species and the growth conditions of the trees. This indicates that at a macro level the material behaviour is strongly influenced by the cellular structure of wood at a micro-level. It is thus natural to try to obtain data providing realistic material descriptions by use of a micro–macro modelling approach.

A typical problem for the engineer, as illustrated in Fig. 2a, is that of wanting the structure involved to consist of well-connected units without discontinuities caused by damage or fracturing. Structural behaviour characterized by a high load-bearing capacity and by ductile (energy-consuming) behaviour at loading is considered to be advantageous. There are a great number of industrial processes, however, in which there is the inverse problem, that of wanting to disconnect solid bodies into small pieces by use of such techniques

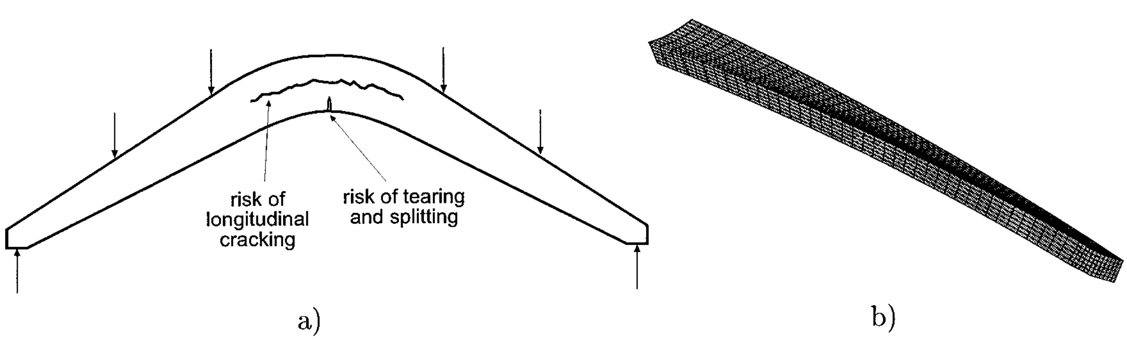

Fig. 2. Illustration of end-user requirements. (a) Load-bearing capacity of an arch beam and risk of failure. (b) Distortion of a structural timber board subjected to moisture variation.

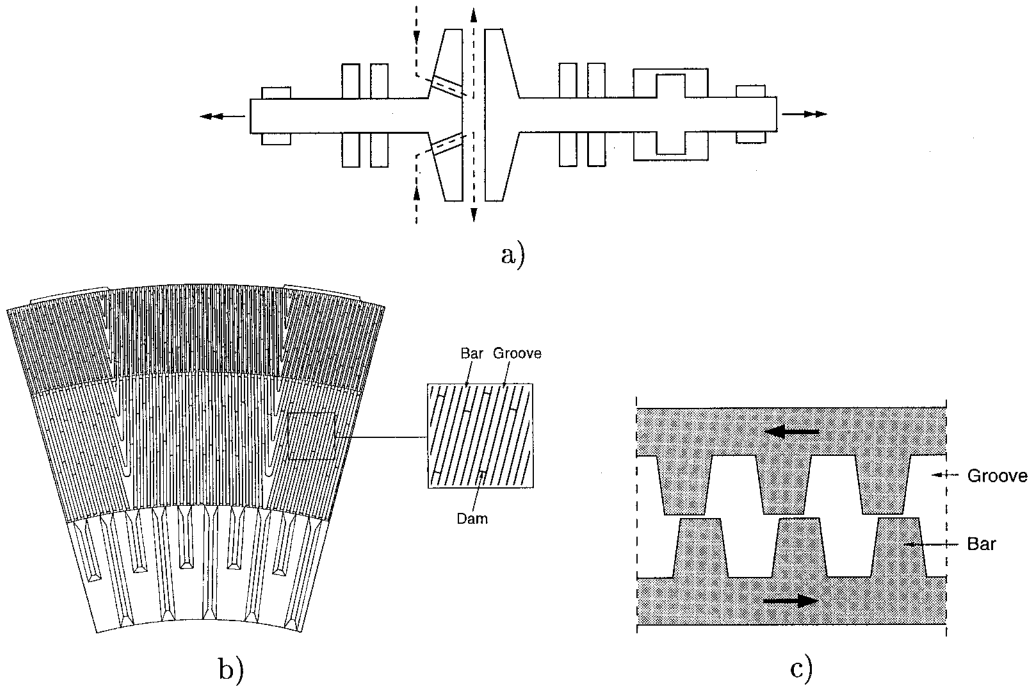

Fig. 3. A refiner for making mechanical pulp. (a) Double-disc refiner. (b) Example of the disc pattern. (c) Loading caused by the moving refiner discs.

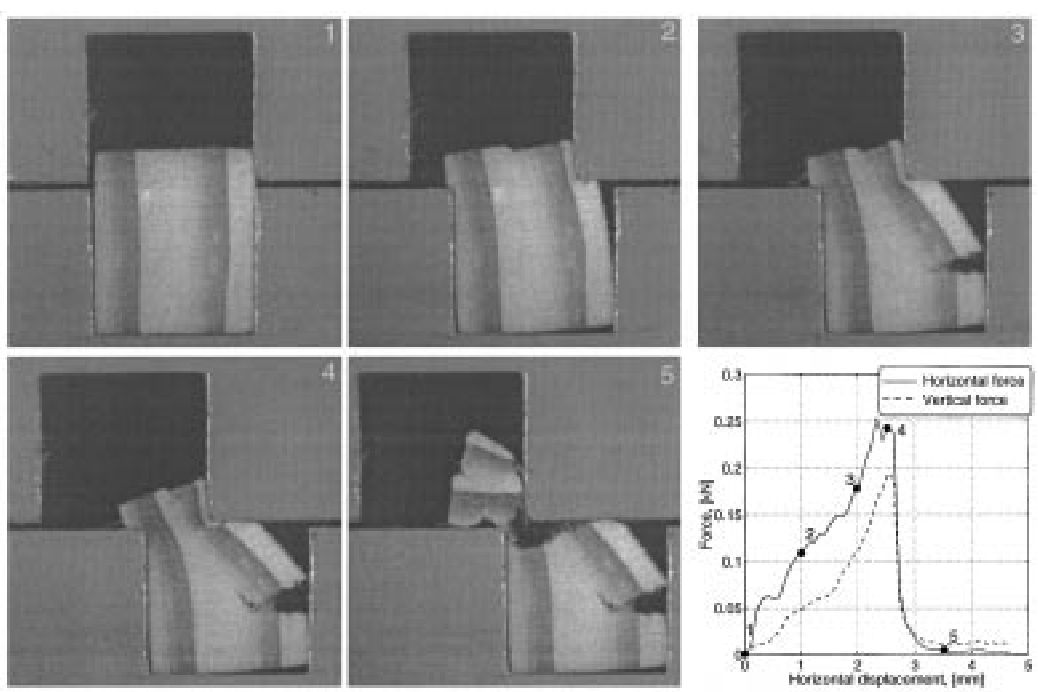

Fig. 4. Illustration of the failure process in a 5 mm high wood specimen bounded by steel grips.

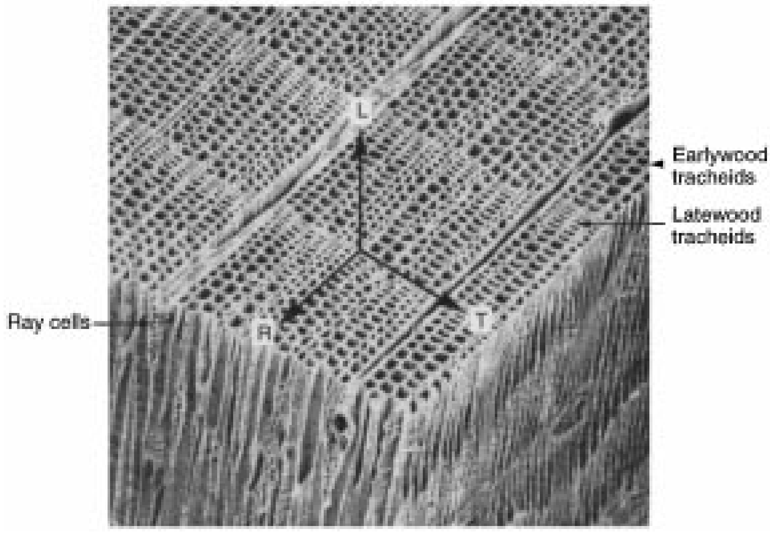

Fig. 5. Cellular structure of softwood. R, T and L denote the radial, tangential and longitudinal directions, respectively. From [9].

as sawing, cutting, grinding or refining. The technique to be used should be as energy-efficient as possible and if crack planes in the material exist they should be utilized. In modelling such processes, the quality of the constitutive models employed and the material data used play a key role in obtaining realistic results in numerical simulations. One such industrial application of great economic importance is the refining process in making mechanical pulp of wood chips. This application is also a good illustration of a challenging numerical problem in a modelling scale between micro and macro. In this type of problem the analysis often involves the need to consider such factors as large deformations, plasticity, damage and fracture.

The objective in producing pulp is to separate the wood material into individual wood fibres and to give them properties suitable for making paper. Pulp manufacturers often refer to this process as refining or defibration. In a refiner wood chips are fed, randomly oriented, into the centre of two rotating discs, see Fig. 3. The chips disintegrate successively, the fibres being separated while moving towards the periphery of the discs. A major drawback of the refining process is its large energy consumption. If the mechanics of the process were better understood, considerable energy could be saved.

In order to better understand the complex loading conditions present in the initial defibration process, an experimental study was carried out [6]. The test setup and the sample dimensions were chosen in view of the geometry of typical refiner segments. The loading conditions resembled those present in the initial defibration process. Fig. 4 illustrates how the material can be deformed and fractured when loaded perpendicular to the grain. The course of the deformation and fracture of the specimen is shown by means of a series of photographs, together with the load-displacement curves recorded. As can be seen, the mechanical behaviour of the specimen is very complex. Its behaviour is characterized by the development of cracks and by large volumetric changes occurring when the earlywood (light colour) is subjected to compression. One can also note that the properties of the latewood (dark colour) differ considerably from those of the earlywood.

Numerical simulations of such processes as sawing, planing, veneer cutting, wood chipping and refining which aim at disintegrating the wooden material require proper constitutive models. Finding such models and properly selected data on the material parameters needed is a challenging task, wood being a highly complex material from a mechanical point of view. Its anisotropy and inhomogeneity, as well as elastic, plastic and fracture mechanical properties need to be considered if numerical simulations are to be realistic.

2. Microstructure of wood

The microstructure of wood is described briefly in the following. For introductory reading about wood, see Refs. [7,8]. A softwood such as spruce contains different cell types. By far the biggest part (90–95%) is composed of long slender cells. These are oriented nearly parallel to the axis of the stem and are about 3–5 mm long and only about 30 μm in cross section. The cells are often almost rectangular in cross section and

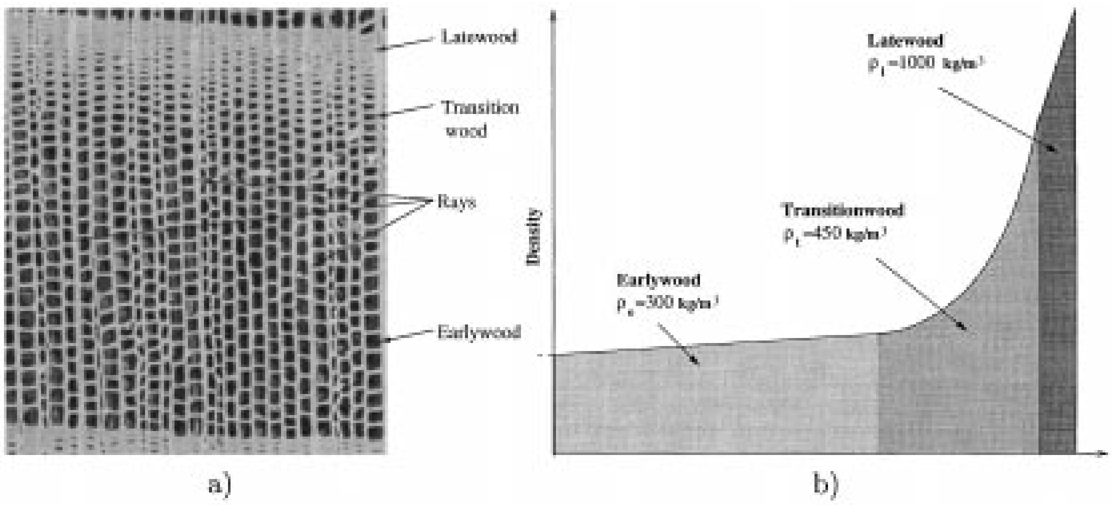

Fig. 6. Characteristics of a growth ring of spruce. (a) Cell structure. (b) Density distribution.

have hollow centres (lumens), being closed at both ends. The main function of these cells is to provide mechanical support to the stem. Because of the manner in which a tree grows and the arrangement of the wood cells within the stem, three principal directions are usually referred to in describing the properties of wood. These are the longitudinal, the radial and the tangential direction, denoted as L, R and T, respectively.

The cellular structure of softwood is illustrated in Fig. 5, showing earlywood, latewood and ray cells. At the level of magnification shown, it is easy to see why wood formed in the latter part of the growing season differs in performance from that formed earlier in the year. The latewood tissue, discernible as the darker-coloured portion of the growth ring, is higher in density than the adjacent parts and is composed of cells of relatively small radial diameter with thick cell walls and small lumens. The cross section of an annual growth ring of wood is shown in Fig. 6, in which different regions of the growth rings can be identified. Each growth ring is composed of three main regions, earlywood, transitionwood and latewood, differing in their density and thus in their mechanical properties. In spruce, the density functions of the earlywood and latewood can be considered as linear, whereas a parabolic density function is suitable for the transitionwood [10].

The cell wall, see Fig. 7, consists mainly of the primary wall (P) and the secondary wall (S), the latter being composed of three layers (S_1, S_2 and S_3). The

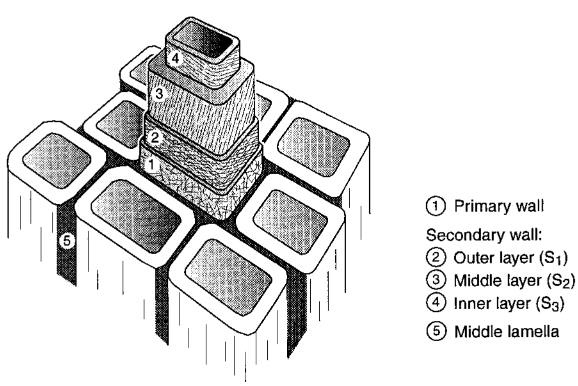

Fig. 7. Schematic drawing of the layers in the cell wall.

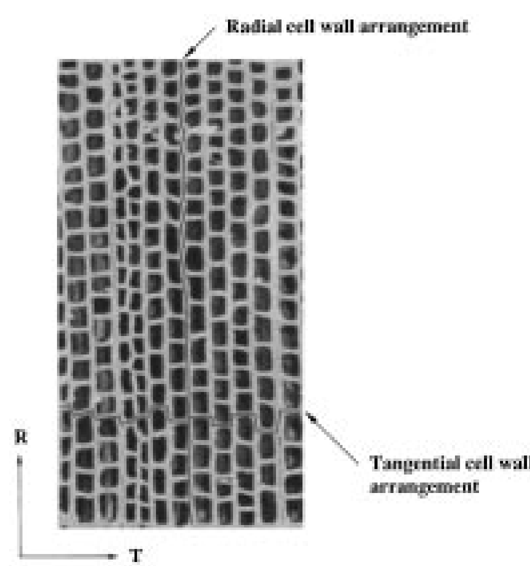

Fig. 8. Cell structure arrangement in the radial and tangential directions.

middle lamellae act primarily as a bonding medium, holding the cells together. The primary and secondary walls can be regarded as fibre-reinforced composites. The layers of these walls consist of cellulose chains located in a hemicellulose and lignin matrix forming thread-like units called microfibrils. The cell-wall layers differ in their thickness, their microfibril orientation and the fractions of their chemical constituents. The microfibril angle of the S_2-layer varies within the tree, especially between juvenile and mature wood, strongly affecting the mechanical properties of the wood. The microfibril angles in the radially and tangentially oriented cell walls may differ, a condition which would also affect the mechanical properties. The larger microfibril angles in the radial cell walls result in an increase in radial stiffness and a decrease in radial shrinkage. Examining the earlywood structure, one can note that the cell arrangement in the radial and the tangential directions differs. In the radial direction, the cells are assembled in fairly straight rows, whereas in the tangential direction they lie in a much more disordered pattern, Fig. 8. This difference in cell arrangement contributes to making the tangential stiffness lower than the radial one. Moreover, the ray cells aligned in the radial direction serve as a reinforcement, resulting in an increase in the stiffness of the wood structure in the radial direction.

The features of the microstructure of wood give rise to a complex mechanical behaviour on a larger scale. In order to improve the linear and nonlinear constitutive models available today for the various scales, account needs to be taken of these features.

3. Introductory remarks on constitutive modelling

Numerical simulations of deformation processes in wood require proper constitutive models. The type of model to be chosen depends on the type of loading and on what environmental effects, such as moisture and temperature variations, which need to be considered. In the simplest case, involving small loads and minor variations in moisture content, it may be sufficient to consider simply the linear elastic and moisture induced strains. In other cases, such as of the drying of wood, it can be necessary to also include in the model mechanosorptive effects and creep [3,5]. Under conditions of very heavy loading, such as in a defibration process, account must be taken of large deformations, plasticity and fracturing. Attending to all these effects in a material such as wood, which with its cellular structure is initially strongly orthotropic, is difficult. In this section various introductory considerations concerning the constitutive modelling will be taken up.

3.1. Elasticity

Wood is a highly anisotropic material. Because of the manner in which a tree grows and the arrangement of the wood cells within the stem, wood can be considered locally as an orthotropic material that possesses three principal directions. Hooke's generalized law for an orthotropic material like wood can be written as

$$\begin{pmatrix} \epsilon_{LL} \\ \epsilon_{RR} \\ \epsilon_{TT} \\ \gamma_{LR} \\ \gamma_{LT} \\ \gamma_{RT} \end{pmatrix} = \begin{pmatrix} \frac{1}{E_L} & -\frac{\nu_{RL}}{E_R} & -\frac{\nu_{TL}}{E_T} & 0 & 0 & 0 \\ -\frac{\nu_{LR}}{E_L} & \frac{1}{E_R} & -\frac{\nu_{TR}}{E_T} & 0 & 0 & 0 \\ -\frac{\nu_{LT}}{E_L} & -\frac{\nu_{RT}}{E_R} & \frac{1}{E_T} & 0 & 0 & 0 \\ 0 & 0 & 0 & \frac{1}{G_{LR}} & 0 & 0 \\ 0 & 0 & 0 & 0 & \frac{1}{G_{LT}} & 0 \\ 0 & 0 & 0 & 0 & 0 & \frac{1}{G_{RT}} \end{pmatrix} \begin{pmatrix} \sigma_{LL} \\ \sigma_{RR} \\ \sigma_{TT} \\ \tau_{LR} \\ \tau_{LT} \\ \tau_{RT} \end{pmatrix} \tag{1}$$

or shorter as

$$\boldsymbol{\epsilon}^e = \mathbf{C}\boldsymbol{\sigma} \tag{2}$$

or as the inverse relationship

$$\boldsymbol{\sigma} = \mathbf{D}\boldsymbol{\epsilon}^e, \quad \mathbf{D} = \mathbf{C}^{-1} \tag{3}$$

where $\boldsymbol{\epsilon}^e$ is the elastic strain vector, $\boldsymbol{\sigma}$ the stress vector and $\mathbf{D}$ the material stiffness matrix. The parameters E_L, E_R and E_T are the moduli of elasticity in the three orthotropic directions and G_{LR}, G_{LT} and G_{RT} are the shear moduli in the respective orthotropic planes. The parameters ν_{LR}, ν_{LT}, ν_{RL}, ν_{RT}, ν_{TL} and ν_{TR} are

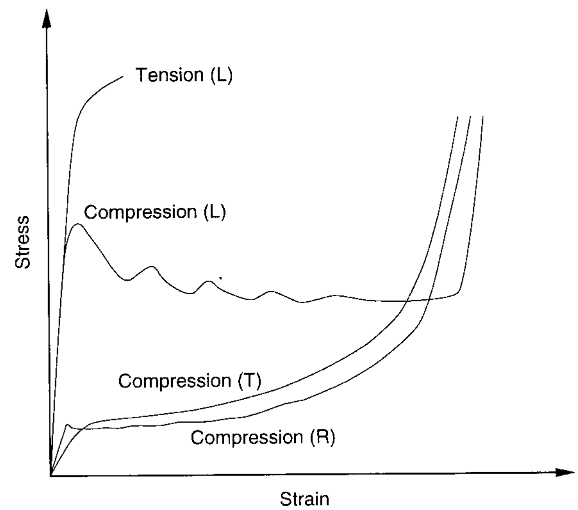

Fig. 9. Typical stress–strain curves for wood loaded in compression in the longitudinal, radial and tangential directions and for tension in the longitudinal direction.

Poisson's ratios. The compliance matrix is symmetric, which implies that

$$\frac{\nu_{RL}}{E_R} = \frac{\nu_{LR}}{E_L}, \quad \frac{\nu_{TL}}{E_T} = \frac{\nu_{LT}}{E_L}, \quad \frac{\nu_{TR}}{E_T} = \frac{\nu_{RT}}{E_R} \tag{4}$$

There are thus nine independent parameters describing the stiffness of an orthotropic material.

The strength and stiffness of wood are considerably greater in the longitudinal than in the perpendicular directions. This can be easily understood on the basis of 90–95% of the fibres being oriented longitudinally. There is also a difference in properties between the radial and tangential directions due to the presence of the rays, as well as to the difference in cellular structure between the radial and tangential directions and the differences of the orientation of the microfibrils on the various sides of the cell. Although the elastic moduli vary with such factors as species, growth conditions, moisture content and temperature, the moduli are generally related in terms of the following ratios [8]:

$$E_L{:}E_L{:}E_L \approx 20{:}1.6{:}1$$

$$G_{LR}{:}\,G_{LT}{:}\,G_{RT} \approx 10{:}9.4{:}1$$

$$E_L{:}G_{LR} \approx 14{:}1 \tag{5}$$

The stiffness and strength properties of wood are strongly dependent on the density, the larger the density, the higher the stiffness and strength. This is obvious since density is a function of the ratio of cell wall thickness to cell diameter. Due to the large difference in cell wall thickness between the earlywood and the latewood, the density of wood varies considerably over a growth ring. Due to the large differences in density between the earlywood and the latewood, the mechanical properties of these two phases of growth differ markedly. Stiffness and strength are considerably higher for the latewood than for the earlywood.

3.2. Nonelastic behaviour

When wood is loaded beyond the elastic region, irreversible changes in the material take place. The limits of proportionality in compression and in tension differ substantially. Above the limit of proportionality, wood behaves in a highly nonlinear way, its behaviour being influenced by several factors, such as density, moisture content, temperature and duration of loading. Fig. 9 shows typical stress–strain curves for wood in a dry condition loaded in different directions in compression and tension. When loaded in compression, the response for the three main directions can be characterized by an initial elastic region, followed by a plateau region and finally a region of rapidly increasing stress. Compression in the tangential direction gives a smooth stress–strain curve which rises gently throughout the plateau, whereas compression in the radial direction tends to give a slightly irregular stress plateau and to be characterized by a small drop in stress after the linear elastic region has been passed. The tangential and the radial yield stresses are about equal. The yield stress in the longitudinal direction is considerably higher than that in the radial and tangential directions and the plateau region is serrated.

For compression perpendicular to the grain, three basic failure patterns can be distinguished, depending on the orientation of the growth rings in relation to the direction of loading, Fig. 10. For radial compression, crushing failure in the earlywood zone occurs. Tangential compression results in a buckling of the growth rings, whereas shear failure often occurs for loading at an angle to the growth rings.

3.3. Fracturing

Eight major cases of crack propagation in wood can be identified [11]. For each of these, fracture can occur in three different modes, mode I representing symmetric opening perpendicular to the crack surface, whereas modes II and III involve antisymmetric shear separations. Cracks in wood can arise then in 24 different principal manners. The resistance to crack propagation is much higher across the grain than in the other directions. The ray cells are of great importance, since in some systems they act as crack initiators, in others crack arrestors. Similarly to compressive loading

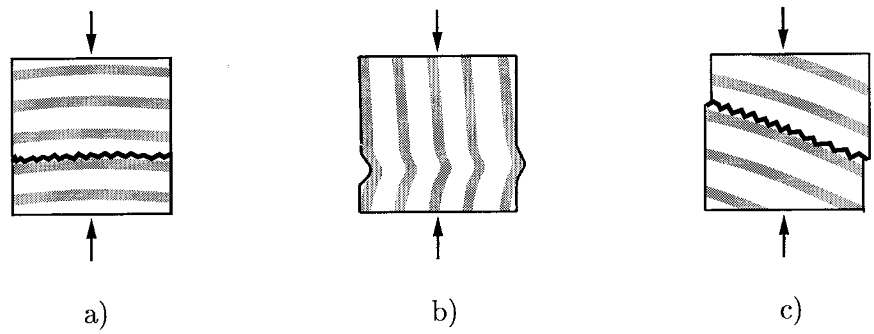

Fig. 10. Failure types in compression perpendicular to the grain [11]. (a) Crushing of earlywood. (b) Buckling of growth rings. (c) Shear failure.

perpendicular to the grain, tensile loading perpendicular to the grain gives rise to three different failure patterns: tensile fracture for radial loading in earlywood; tensile failure in the wood rays for tangential loading; and shear failure along a growth ring when loading is at an angle to the growth rings. At the microstructural level, the crack propagation for mode I loading can occur in two different ways. The crack may advance across the cell walls (cell-wall breaking), Fig. 11a, or it may propagate between two adjacent cells close to the middle lamellae (cell-wall peeling), Fig. 11b.

3.4. Cell structure instabilities

The behaviour of the cell structure was studied with the aid of SEM micrographs through applying both uniaxial and biaxial deformations to wood specimens [12]. The load cases involved prescribed displacements in terms of tension, compression, shear and a combination of compression and shear. It was found that with radial compression the cell structure collapsed due to instability, even at rather moderate applied strains, Fig. 12a. The collapse was localized to the first cell rows of the earlywood. As the deformation process continued, the cell structure of the earlywood continued to collapse towards the latewood, until almost all of the earlywood cells had collapsed. Even with very large applied deformations, however, the deformations of the latewood were small, and no cell-wall buckling occurred. In tensile loading, an unstable crack propagation developed, the crack being found to propagate through the cell walls of the earlywood and to then follow a ray in the latewood, Fig. 12b. Shear loading in the radial–tangential plane led to large deformations in the first cell rows of the earlywood but to no visible deformations in the latewood. Failure in the form of a shear crack developed in the boundary between earlywood and latewood. At moderate shear strains, the largest deformations occurred in the middle of the earlywood region, Fig. 12c. Combined compression and shear loading resulted in large localized strains in the first cells of the earlywood region, without any visible deformations in the latewood. Due to a large deformation zone being formed, the material lost much of

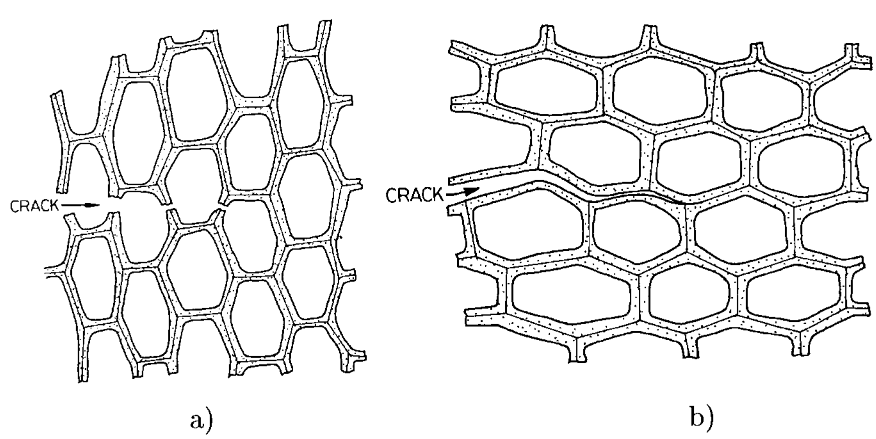

Fig. 11. Crack propagation at the microstructural level for mode I loading [11]. (a) Cell-wall breaking. (b) Cell-wall peeling.

its shear strength, although still retaining its compressive strength, Fig. 12 d.

4. Micro–macro modelling of wood properties

Different approaches to deriving the properties of wood by modelling its cell structure have been attempted earlier [11,13–15]. In this section, means of determining the equivalent stiffness and shrinkage properties of wood through use of a micro-mechanical approach [6,16] will be outlined. Some of the ideas presented in the earlier studies are adopted here. A homogenization method is employed in which the basic equations are solved by use of the finite element method. A scheme showing the various steps involved in determining the equivalent properties is presented in Fig. 13.

In the first step, the equivalent properties of the different cell wall layers were calculated from the properties of cellulose, hemicellulose and lignin. The geometry of the microfibrils was simplified to their being composed of repetitive units, allowing homogenization theory to be applied. Microfibril models involving different fractions of the chemical constituents were created for representing the different layers of the cell wall (Fig. 14). The equivalent properties were then determined from these microfibril models by use of a homogenization approach and the finite element method. Transformations of the material stiffnesses were made so as to align the local 1-, 2- and 3- directions of the microfibril material with the global L-, R- and T-directions. For each layer of the cell wall, differ-

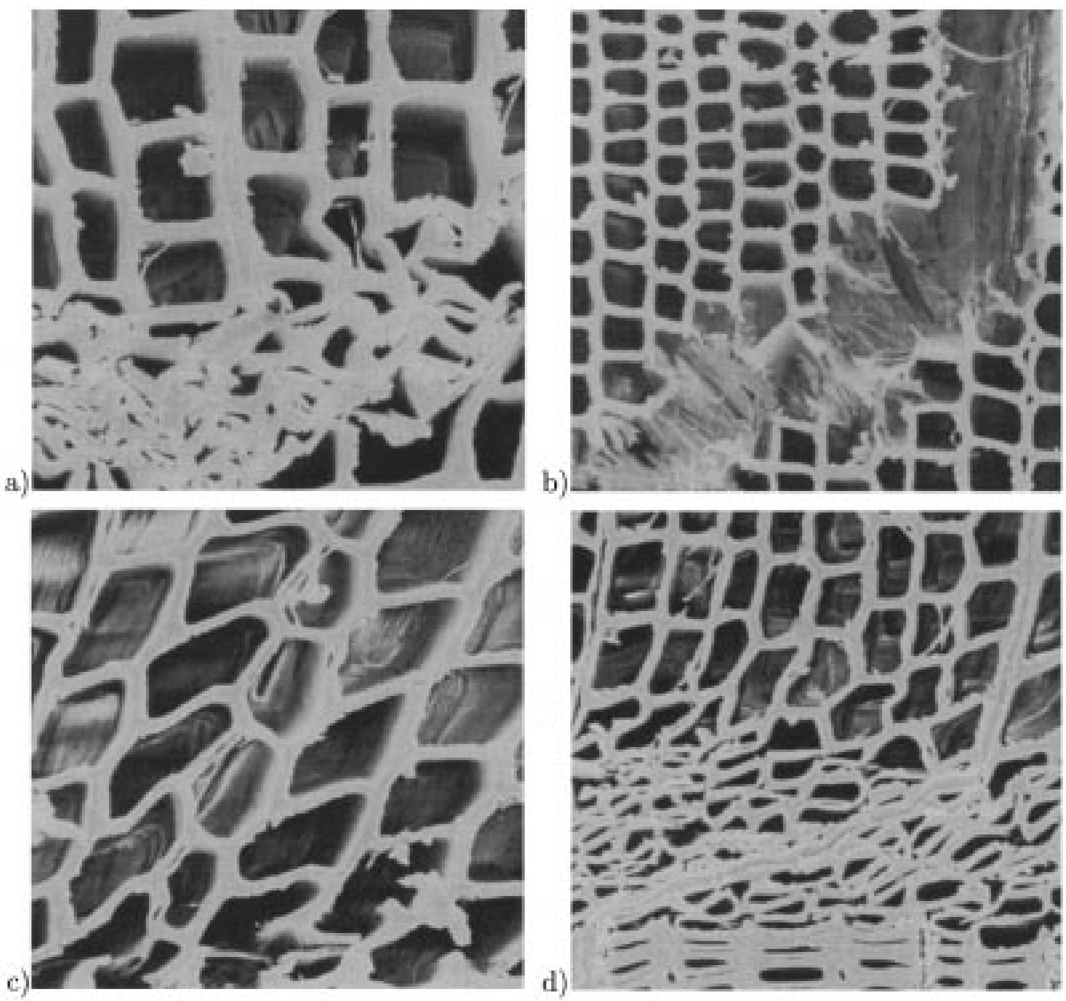

Fig. 12. Cell structure deformations at failure under various loading conditions. (a) Compression; (b) tension; (c) shear; and (d) combined shear and compression.

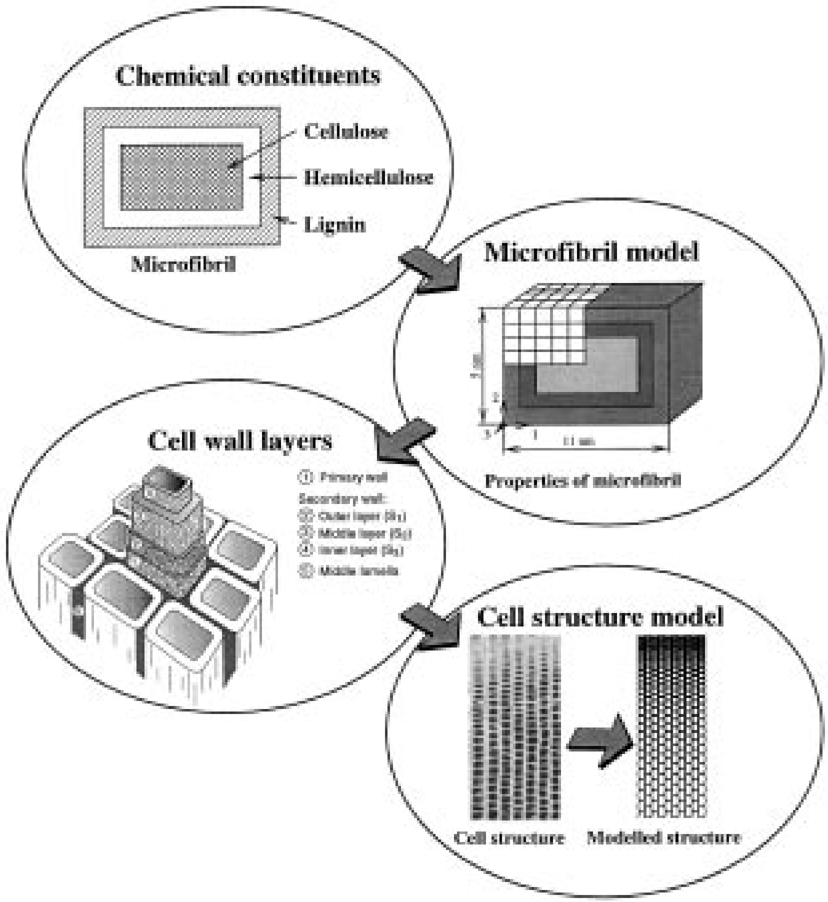

Fig. 13. Modelling scheme.

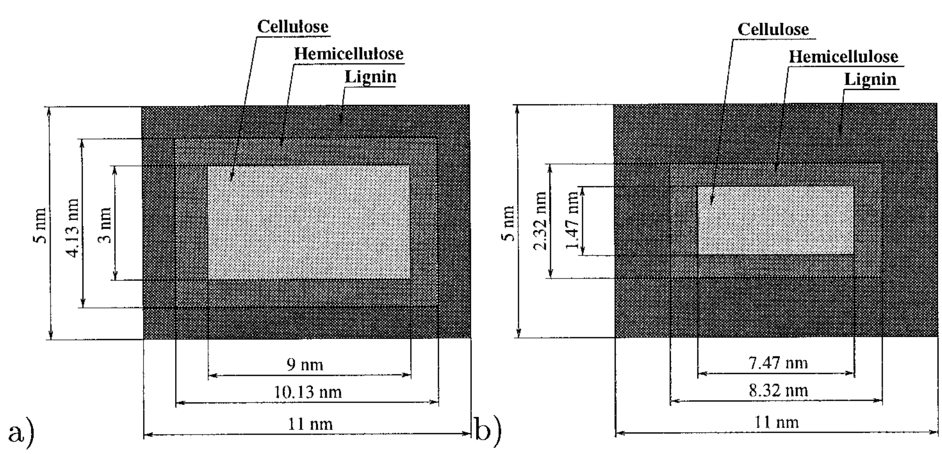

Fig. 14. Assumed geometry of the microfibril cross sections. (a) For the the S_2- and S_3-layers. (b) For the M-, P- and S_1-layers.

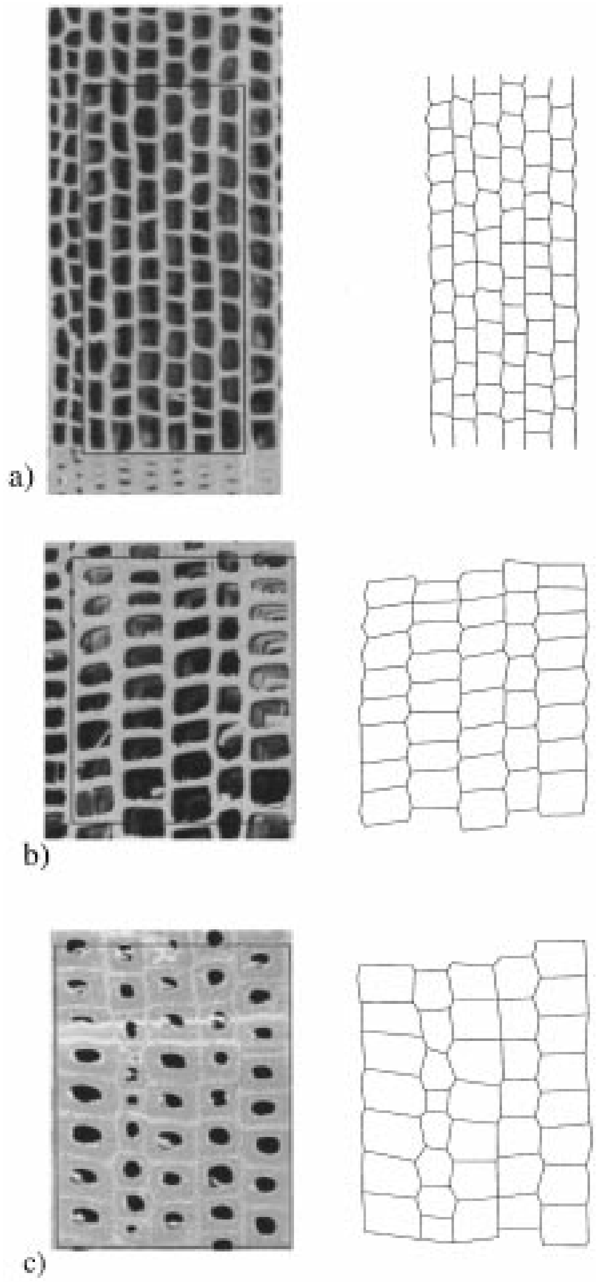

Fig. 15. Micrographs of the real cell structures (left) and the modelled structures (right). (a) Earlywood. (b) Transitionwood. (c) Latewood.

ent material properties were defined and separate transformations corresponding to the microfibril orientation of the layers were carried out.

The second step of the modelling was to determine the equivalent properties of the wood structure. The modelling of the wood cell structures was approached in two different ways. One was to model real cell structures as selected from micrographs, these cell structures being assumed to be representative of the cell structures in the wood generally. Three regions of the growth ring were selected from micrographs as being representative of spruce. These included one region with a typical earlywood cell structure, one with a typical transitionwood structure and one with a typical latewood structure, see Fig. 15. The geometrical models obtained from the micrographs were extended in the longitudinal direction to obtain three-dimensional structures that were meshed with eight-node composite shell elements. Such a composite formulation makes it possible to define several different material layers in an element [17]. The thicknesses of the cell walls were determined from the average densities for the respective region at 300, 450 and 1000 kg/m^3 and for a cell wall bulk density of 1500 kg/m^3.

Another, simpler approach that was employed was to model the cell structure on the basis of a five-parameter cell structure model having properties as close as possible to those of the real cell structure. Three-dimensional cell structures of complete growth rings were modelled as being composed of irregular hexagonal cells (Fig. 16a). The geometry of the cell structures was based on micrographs and on microstructural measurements. Assuming the shape of the cells as shown in Fig. 16a, the cell structure of a growth ring can be modelled through appropriate variations in the parameters involved.

Knowing the variations in density over the growth ring and the radial widths of the cells, a model of a complete growth ring can be obtained, see Fig. 16b. The density functions in the three regions of the growth ring were modelled as shown in Fig. 6b. In the earlywood region the density was assumed to show a slight linear increase, causing the cell wall thickness to increase slightly, whereas the radial cell width was assumed to be constant. In the transitionwood, the density was assumed to increase rapidly, causing the cell wall thickness to increase accordingly and the radial cell width to decrease. In the latewood, finally, the density was assumed to increase linearly and the cell wall thickness to likewise increase, the radial cell width being assumed to be constant. At each side of the cell-structure model, rays with a stiffness equal to that of an earlywood cell were included.

Since the models of complete cell structures of trees or boards consisting of several growth rings become very large, they cannot be directly modelled. However, the average stiffness and shrinkage properties of growth rings with different radial widths and different average densities can be determined by use of a homogenization procedure and the finite element method. Parameters obtained in this way can then be used in various analyses.

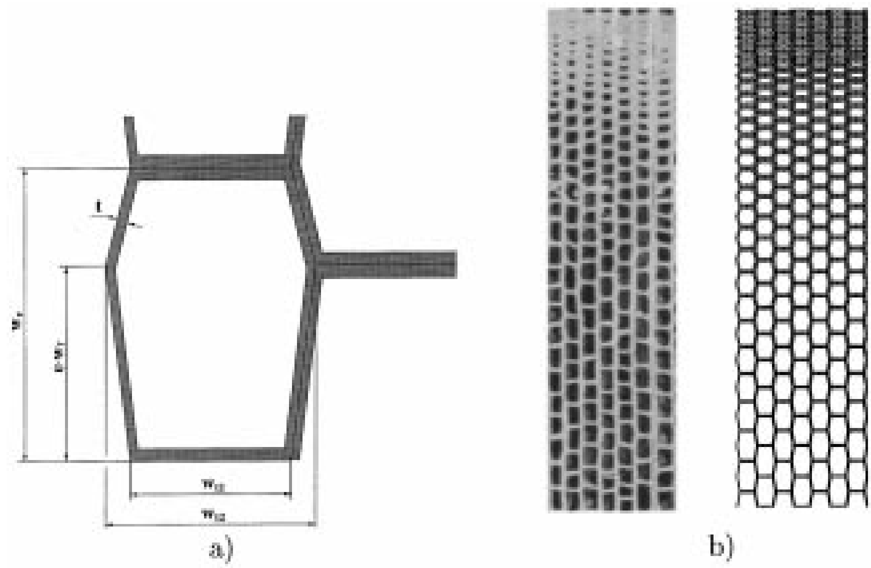

Fig. 16. Simplified modelling of a growth ring. (a) Single-cell geometry. (b) Photographed and modelled cell structures.

5. Homogenization by use of FEM

The basic idea of homogenization is to average the behaviour of a material of complex periodic microstructure through replacing the material by an equivalent homogeneous continuum. With the aid of a homogenization procedure and the finite element method, the constitutive global behaviour of the corresponding heterogeneous material can be derived. A material with a periodic microstructure has properties that vary in a repetitive pattern throughout the body. In the homogenization procedure, a representative volume element of the material, referred to as the base cell, is defined. If the material has a periodic structure, the material can be divided into equal substructures, the base cell being chosen as one of the periods of the structure.

Periodic structures are to be found at different levels in wood. The cell-wall layers are composed of microfibrils consisting of cellulose chains in a matrix material of hemicellulose and lignin. Everywhere in the cell wall the microfibrils are assumed to be similar in size and shape, forming a periodic structure. At this level the microfibril can be regarded as the base cell. At a higher

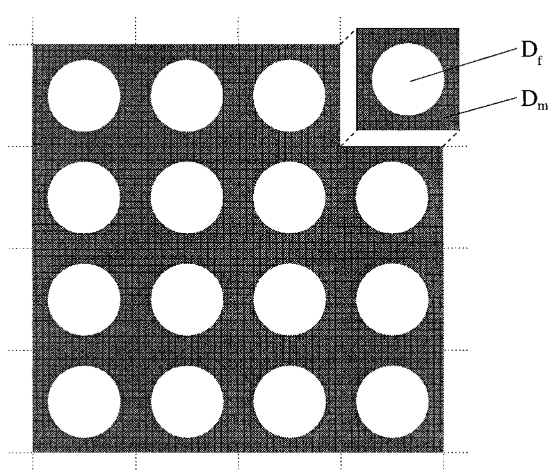

Fig. 17. A periodic structure composed of two different materials, D_f and D_m. The representative volume element is shown in the upper right.

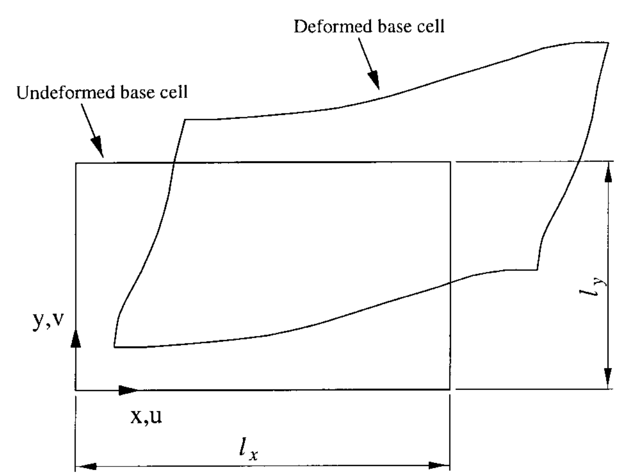

Fig. 18. Two-dimensional base cell in an undeformed and a deformed state.

wood-structure level, a portion of the growth ring can be regarded as a periodic structure as well.

In this section, a homogenization procedure using the finite element method is described. It is used to derive the equivalent smeared properties of the material from the microstructure. The microstructure of the body is assumed to be periodic and the material to be composed of subcells of equal shape and identical material properties in each subcell. A subcell can be selected then as a representative volume element, one that is repeated throughout the body, as shown in Fig. 17. Only certain basic features of the homogenization method will be outlined in this paper. For further information on the subject, see Ref. [18], for example.

Each representative volume element of volume Ω in the body has the same shape and same material properties $D_{ijkl} = D_{ijkl}\ (x,\ y,\ z)$ with respect to the local coordinate systems. In both undeformed and deformed configurations, adjacent base cells must always fit together at the boundaries. Moreover, for a homogeneous stress-field, cells lying far from the boundaries are all subjected to the same loading conditions and deform in the same manner. The possible shapes that the cells in the undeformed and the deformed configurations can assume are therefore confined in such a way that the boundaries of opposing sides of a base cell always possess the same shape. The two-dimensional case in Fig. 18 shows a rectangular base cell in an undeformed and a deformed state, together with the material coordinates $(x,\ y)$, the displacements $(u,\ v)$ and the lengths of the sides $(l_x,\ l_y)$.

Due to the opposing boundary surfaces of the base cells being identical in shape and size, the relations between the displacements of the boundaries can be readily established. For simplicity, it is assumed that in an undeformed state the base cell is a right prism having the volume $\Omega = l_x l_y l_z$. The deformation state with respect to the boundaries can then be expressed by the matrix $\mathbf{A}$,

$$\mathbf{A} = \begin{bmatrix} \dfrac{u(l_x,y,z) - u(0,y,z)}{l_x} & \dfrac{u(x,l_y,z) - u(x,0,z)}{l_y} & \dfrac{u(x,y,l_z) - u(x,y,0)}{l_z} \\ \dfrac{v(l_x,y,z) - v(0,y,z)}{l_x} & \dfrac{v(x,l_y,z) - v(x,0,z)}{l_y} & \dfrac{v(x,y,l_z) - v(x,y,0)}{l_z} \\ \dfrac{w(l_x,y,z) - w(0,y,z)}{l_x} & \dfrac{w(x,l_y,z) - w(x,0,z)}{l_y} & \dfrac{w(x,y,l_z) - w(x,y,0)}{l_z} \end{bmatrix} \tag{6}$$

The columns j in $\mathbf{A}$ refer to the two bounding surfaces originally normal to the x_j-direction. Since the outward normals n_j of the base cell are of opposite sign on opposing sides, the tractions $t_i = \sigma_{ji} n_j$ are anti-periodic, meaning that

$$t_i(l_x,y,z) = -t_i(0,y,z)$$

$$t_i(x,l_y,z) = -t_i(x,0,z)$$

$$t_i(x,y,l_z) = -t_i(x,y,0) \tag{7}$$

The equilibrium equation can thus in a case with no body forces be written as

$$\frac{\partial \sigma_{ji}}{\partial x_j} = 0 \quad \text{in } \mathbf{\Omega}$$

$$t_i = \sigma_{ji} n_j \quad t_i \text{ anti-periodic on } \mathbf{\Gamma}$$

$$u_i \quad \text{periodic on } \mathbf{\Gamma} \tag{8}$$

over the base cell volume $\mathbf{\Omega}$ with cyclic boundary conditions on the boundary surface $\mathbf{\Gamma}$. The weak formulation of Eq. (8), in which the weighting functions are set equal to the displacements u_i, becomes

$$\int_{\mathbf{\Omega}} \frac{\partial u_i}{\partial x_j} \sigma_{ij}\, \mathrm{d}\mathbf{\Omega} = \int_{\mathbf{\Gamma}} u_i t_i\, \mathrm{d}\mathbf{\Gamma} \tag{9}$$

with use of proper boundary constraints on the displacements on $\mathbf{\Gamma}$.

If the boundary $\mathbf{\Gamma}$ is split into three parts $\mathbf{\Gamma} = 2\mathbf{\Gamma}_1 + 2\mathbf{\Gamma}_2 + 2\mathbf{\Gamma}_3$ where $2\mathbf{\Gamma}_j$ contains the two surfaces normal to the x_j-direction, Eq. (9) can be written as

$$\int_{\mathbf{\Omega}} \frac{\partial u_i}{\partial x_j} \sigma_{ij}\, \mathrm{d}\mathbf{\Omega} = \sum_{j=1}^{3} \Delta u_i \int_{\mathbf{\Gamma}_j} t_i\, \mathrm{d}\mathbf{\Gamma} \tag{10}$$

where $\mathbf{\Gamma}_j$ is one of the two surfaces normal to the x_j-direction. According to Eq. (6),

$$\Delta u_i = A_{ij} l_{\langle j \rangle} \tag{11}$$

where the bracketed index indicates that the summation convention is not applied and where $l_1 = l_x$, $l_2 = l_y$ and $l_3 = l_z$. Using Eq. (11) one can write Eq. (10) as

$$\int_{\mathbf{\Omega}} \frac{\partial u_i}{\partial x_j} \sigma_{ij}\, \mathrm{d}\mathbf{\Omega} = A_{ij} l_{\langle j \rangle} \int_{\mathbf{\Gamma}_{\langle j \rangle}} t_i\, \mathrm{d}\mathbf{\Gamma} \tag{12}$$

Still assuming the base cell to be a right prism in the undeformed state, the average stresses (tractions) on the boundary surfaces can be defined as

$$B_{ij} = \frac{1}{\mathbf{\Gamma}_{\langle i \rangle}} \int_{\mathbf{\Gamma}_{\langle i \rangle}} t_j \, \mathrm{d}\mathbf{\Gamma} \tag{13}$$

where $\mathbf{\Gamma}_{\langle i \rangle}$ refers to a surface normal to the x_i-direction. Eq. (12) can then be rewritten as

$$\int_{\mathbf{\Omega}} \frac{\partial u_i}{\partial x_j} \sigma_{ij} \, \mathrm{d}\mathbf{\Omega} = \mathbf{\Omega} A_{ij} B_{ij} \tag{14}$$

where the base cell volume $\mathbf{\Omega} = l_x l_y l_z$.

For small deformations, the average strains can be defined as

$$\bar{\epsilon}_{ij} = \frac{1}{2}(A_{ij} + A_{ji}) \tag{15}$$

and, correspondingly, the average stresses as

$$\bar{\sigma}_{ij} = \frac{1}{2}(B_{ij} + B_{ji}) \tag{16}$$

The expressions for the average strains and stresses are then substituted into Eq. (14), yielding

$$\int_{\mathbf{\Omega}} \frac{\partial u_i}{\partial x_j} \sigma_{ij} \, \mathrm{d}\mathbf{\Omega} = \mathbf{\Omega} \bar{\epsilon}_{ij} \bar{\sigma}_{ij} \tag{17}$$

A linear elastic material model including moisture-induced shrinkage is chosen here as an example of a constitutive equation. The constitutive relations for the base cell are then

$$\sigma_{ij} = D_{ijkl}(\epsilon_{kl} - \epsilon^{s}_{kl}) \tag{18}$$

The shrinkage strains ϵ^{s}_{kl} can be expressed as

$$\epsilon^{s}_{kl} = \alpha_{kl} \Delta w \tag{19}$$

where α_{kl} are the shrinkage coefficients and Δw is the change in moisture content. Due to the inhomogeneous material properties of the base cell, both D_{ijkl} and α_{kl} can vary markedly in space. In addition, if local cavities appear in the base cell, the material stiffness as represented by D_{ijkl} is set to zero. The material within the base cell is assumed to be replaced then by an equivalent fictitious material of constant stiffness and shrinkage properties denoted as $\bar{D}_{ijkl}$ and $\bar{\alpha}_{kl}$, respectively.

With constant moisture content, the constitutive relation becomes

$$\bar{\sigma}_{ij} = \bar{D}_{ijkl} \bar{\epsilon}_{kl} \tag{20}$$

having the inverse relationship

$$\bar{\epsilon}_{ij} = \bar{C}_{ijkl} \bar{\sigma}_{kl} \tag{21}$$

A simple way of defining the constitutive parameters in Eqs. (20) and (21) is to choose six elementary cases of stress states that correspond to the respective stress tensors

$$\begin{bmatrix} 1 & 0 & 0 \\ 0 & 0 & 0 \\ 0 & 0 & 0 \end{bmatrix} \quad \begin{bmatrix} 0 & 0 & 0 \\ 0 & 1 & 0 \\ 0 & 0 & 0 \end{bmatrix} \quad \begin{bmatrix} 0 & 0 & 0 \\ 0 & 0 & 0 \\ 0 & 0 & 1 \end{bmatrix}$$

$$\begin{bmatrix} 0 & 1 & 0 \\ 1 & 0 & 0 \\ 0 & 0 & 0 \end{bmatrix} \quad \begin{bmatrix} 0 & 0 & 1 \\ 0 & 0 & 0 \\ 1 & 0 & 0 \end{bmatrix} \quad \begin{bmatrix} 0 & 0 & 0 \\ 0 & 0 & 1 \\ 0 & 1 & 0 \end{bmatrix} \tag{22}$$

Note that, due to the unit stress value found for each of the six cases in Eq. (22), one can identify that

$$\bar{C}_{ijkl} = \bar{\epsilon}_{ij} \quad \text{for} \quad k = l$$

$$\bar{C}_{ijkl} = \bar{C}_{ijlk} = \frac{1}{2}\bar{\epsilon}_{ij} \quad \text{for} \quad k \neq l \tag{23}$$

For the shrinkage parameters, the averaging can be performed in a similar way. Prescribing for a seventh case that $\bar{\sigma}_{\mathrm{kl}} = 0$ for all k and l and that $\Delta w = 1$ yields the relation

$$\bar{\alpha}_{kl} = \bar{\epsilon}_{kl} \tag{24}$$

Thus the constitutive parameters can be identified on the basis of seven elementary cases involving either prescribed average tractions or a change in moisture content.

5.1. Numerical example

A comparison of the irregular hexagonal cell structure model and the model based on the properties of real cell structures was performed, ray cells being included in both models. The elastic stiffness and shrinkage properties of a growth ring obtained by use of the respective models were compared, an average density of 400 kg/m^3 and a microfibril angle in the S_2-layer of 10°, being employed. Table 1 shows the comparison of the two models, together with typical measured values of spruce, as obtained from the experiments reported in [10] and from literature [19,20]. A comparison of the stiffness values obtained shows both models to provide results close to the measured data, for both models the values of the elastic stiffness parameters lying the interval indicated by the measurements. However, for the models as compared with the experimental results, the radial stiffness was found to be somewhat higher than the other stiffness parameters and the difference between the radial and tangential shrinkage to be smaller. This may be due to the geometry or the material properties of the radial and the

Table 1
Elastic stiffness and shrinkage parameters obtained from the two models compared with measurements

Parameter	Irregular hexagonal model	Model based on real structures	Measurements [10,19,20]
E_L (MPa)	14,300	13,200	6000–25,000
E_R (MPa)	1120	1110	700–1200
E_T (MPa)	556	590	400–900
G_{LR} (MPa)	605	703	600–700
G_{LT} (MPa)	594	555	500–600
G_{RT} (MPa)	35.0	22.0	20.0–70.0
ν_{LR}	0.049	0.048	0.02–0.050
ν_{LT}	0.022	0.019	0.01–0.025
ν_{RT}	0.11	0.19	0.20–0.35
α_L	0.00635	0.00414	0.001–0.006
α_R	0.236	0.177	0.13–0.25
α_T	0.294	0.194	0.25–0.40

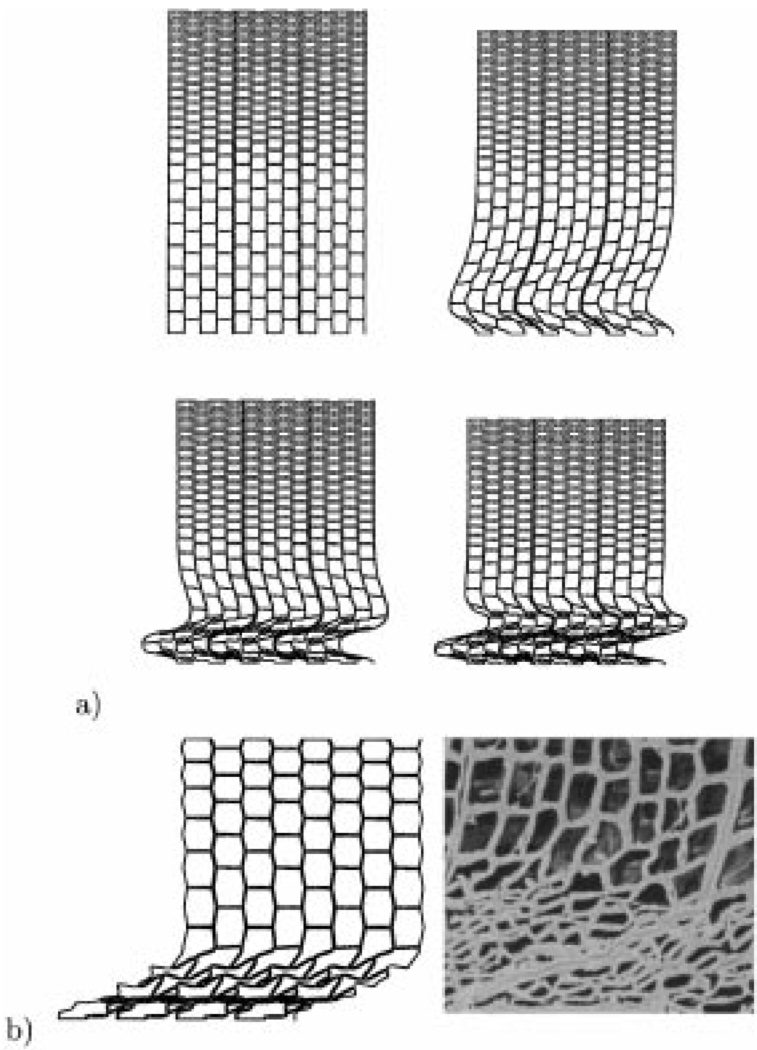

Fig. 19. Numerical simulation of cell structure deformations. (a) Sequence for pure radial compression. (b) Combined shear and compression compared with experimental result.

tangential cell walls differing. For further details concerning the computations, see [10].

The homogenization procedure can also be used for determining the equivalent global material properties in the case of local buckling of the cell walls within the growth rings. An example in which nonlinear geometric effects have been considered is shown in Fig. 19. It is interesting to note that a phenomenon which at a macro level best is described by a nonlinear material behaviour is often very much dominated at a micro level by nonlinear geometrical effects.

6. Constitutive modelling of wood for initial defibration applications

6.1. Introduction

Two main approaches to modelling the wooden material can be taken when numerical analyses of initial defibration processes are to be performed. One approach is to use continuum models based on the average material properties. The other approach is to develop models of the cellular microstructure in which the individual fibres are modelled. The latter approach is the most general one and possesses a higher degree of resolution. It has the disadvantage, however, of yielding huge models which, unless very small pieces of wood are studied, are difficult to handle with the computer resources available today. Although a continuum modelling approach allows the deformation and fracturing of large wood pieces to be analysed [6], it does not permit the deformation and fracturing of the individual fibres to be studied. The continuum approach seems to be the most suitable for simulating the initial breakdown of the wooden chips in a refiner. At later stages of the defibration process, modelling at the microstructural level is needed in order to analyse the deformation process for the individual fibres.

In this section a continuum modelling approach is presented and discussed. The approach is useful in analysing and simulating different defibration processes, mechanical pre-treatment types, loading-mode types, directions of loading, loading rates, etc. Some numerical examples adopting this modelling approach are given in Section 7.

6.2. Modelling approach

The most important conclusion to be drawn from the experimental investigation [6] is that, in studying initial defibration processes account must be taken of the inhomogeneities of the material. The experiments clearly demonstrate there to be differences in mechanical properties between earlywood and latewood, see Fig. 4. These differences must be taken into account. In addition, the experiment shows that the mechanical behaviour of wood loaded perpendicular to the grain is very complex. Characteristic of the behaviour of the material, when it is subjected to compression, is the development of cracks and of large volumetric changes in the earlywood. In order to perform proper modelling of the initial defibration processes, consideration must thus be given to the following material characteristics:

- the strong variation in the material properties within each growth ring;
- the nonlinear inelastic response of earlywood subjected to compression perpendicular to the grain;
- the fracture behaviour of the material.

The variation of the material properties is taken into account by dividing the wood in the growth ring into at least two zones of both earlywood and of latewood. The earlywood zones can be further subdivided in the radial direction into several layers that differ slightly in their stiffness and strength properties. The strain localization arising when earlywood is subjected to compression must be captured in an adequate way.

A crushable foam model is used to model the behaviour of earlywood. Foams are characterized by their ability to deform volumetrically when subjected to compression, a deformation due to cell-wall buckling processes in the microstructure, similar to the observed behaviour of earlywood. In light of the increasing structural use of foams, various constitutive models have been developed [17,21,22]. The model employed in this study is similar to that considered in [21] and is based on nonassociated compressible plasticity. For latewood it was found to be sufficiently accurate to assume linear elastic behaviour as long as no cracks had developed.

Fracture of the material is taken into account by use of a fictitious crack model. The fracturing properties are projected onto distinct cracking surfaces associated with softening stress–relative displacement relations. This fictitious crack model is implemented in the finite element simulations by introducing special crack elements between the solid elements.

There is a certain directional dependence within the transverse plane of wood. The stiffness ratio of the radial to the tangential direction is normally between about 1.5 and 2. This stiffness ratio is based, however, on conditions in which the material is considered as a continuum, the differences between earlywood and latewood not being taken into account.

It should be noted that the differences normally observed between the radial and the tangential directions, concern only the linear elastic part of the material behaviour and thus only before the radial cell walls have buckled. In the present applications, in

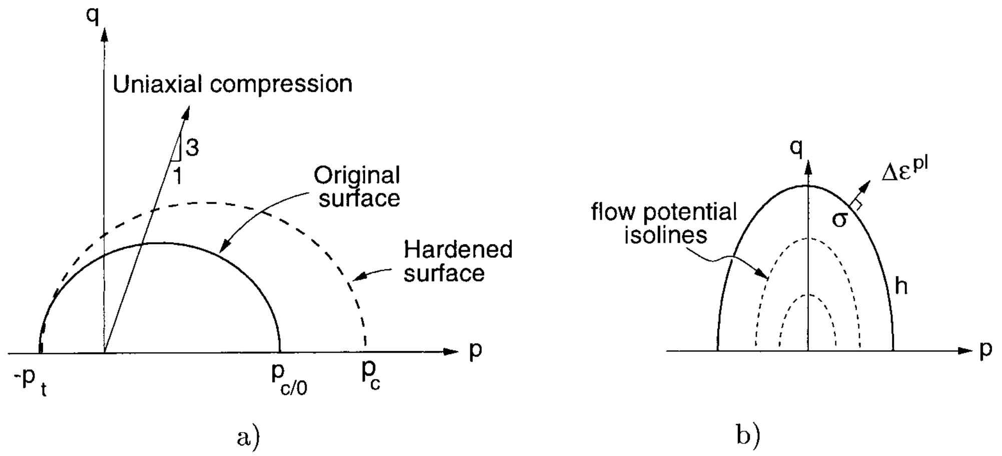

Fig. 20. Characteristics of the foam model. (a) Yield surface. (b) Plastic potential surface.

which earlywood is loaded far beyond the linear elastic region, these differences are probably not particularly important for the overall behaviour of the material. This suggests that use of an isotropic foam model can provide quite reasonable results when loading perpendicular to the grain is analysed. For more arbitrary loading conditions and loading directions orthotropic foam models should be used, see e.g. Ref. [22]. In the two sections that follow the foam plasticity model and the fictitious crack model, respectively, are presented.

6.3. Isotropic foam plasticity model

The isotropic foam plasticity model, see e.g. [17,21] is rather well-established. In the following, the basics of the model as it was employed in the present study are presented. The behaviour in the elastic region is assumed to be linear. The yield surface is defined in terms of the equivalent pressure stress p and the Mises equivalent stress q, defined as

$$p = -\frac{1}{3}\sigma_{kk} \tag{25}$$

$$q = \sqrt{\frac{3}{2}S_{ij}S_{ij}} \tag{26}$$

where σ_{ij} are the components of the Cauchy stress tensor and S_{ij} are the deviatoric stress components as given by

$$S_{ij} = \sigma_{ij} + pI_{ij} \tag{27}$$

The yield surface is defined as

$$F = \sqrt{\left(\frac{p_t - p_c}{2} + p\right)^2 + \left(\frac{q}{M}\right)^2} - \frac{p_c + p_t}{2} = 0 \tag{28}$$

where p_t is the strength of the material in hydrostatic tension and $p_c = p_c(\epsilon_{vol}^{pl})$ is the yield stress in hydrostatic compression as a function of the volumetric plastic strain. M is a constant computed from the yield stress in uniaxial compression according to

$$M = \frac{\sigma_0}{\sqrt{p_t p_{c/0} - \frac{1}{3}\sigma_0(p_t - p_{c/0}) - \frac{1}{9}\sigma_0^2}} \tag{29}$$

where σ_0 is the initial yield stress in uniaxial compression and $p_{c/0}$ is the initial value of p_c. The yield criterion of Eq. (28) defines an elliptical yield surface in the p–q plane. The yield surface intersects the p-axis at $-p_t$ and p_c. The compressive strength, p_c, increases when the material is compacted, whereas p_t remains fixed throughout any plastic deformation process. The yield surface is illustrated in Fig. 20a. In the deviatoric plane the yield surface is a circle. The strength in hydrostatic tension p_t remains fixed, whereas the compressive strength p_c evolves as a result of compaction of the material. This is modelled by a piecewise linear function.

Potential flow is assumed, the flow rule being written as

$$\Delta\epsilon_{ij}^{pl} = \Delta\lambda\frac{\partial h}{\partial\sigma_{ij}} \tag{30}$$

where $\Delta\epsilon^{pl}$ is the plastic strain increment, $\Delta\lambda$ the plastic multiplier, and h the flow potential, given by

$$h = \sqrt{\frac{9}{2}p^2 + q^2} \tag{31}$$

A geometrical representation of this flow potential is shown in Fig. 20b. The flow potential gives a direction of flow that is identical to the stress direction for radial

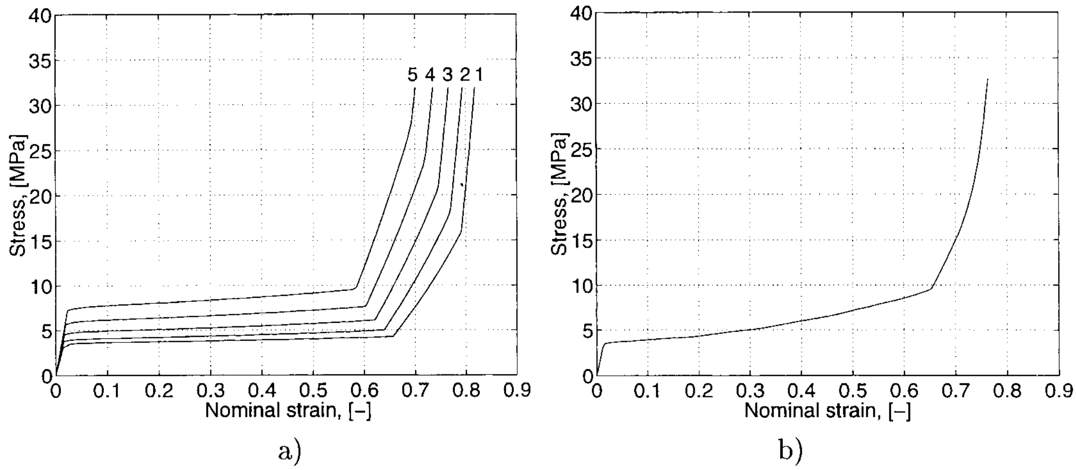

Fig. 21. Characteristics of the foam model. (a) Stress-strain curves for the five different earlywood layers. (b) Response of the complete earlywood zone when loaded in the radial direction.

paths. Thus loading in any principal direction causes no deformation in the other directions.

In the present study, the earlywood zone is divided into five equally thick layers differing slightly in their stiffness and strength properties. This is done to at least partly capture the strain localization that occurs when earlywood is loaded in compression in the radial direction. The layers are referred to as earlywood 1–5, earlywood 1 being the weakest layer, representing the material formed in the early spring, and earlywood 5 being the strongest layer, representing the transition zone. In Fig. 21a the adopted compressive response in the form of stress–strain curves for the five different earlywood layers is shown. The response for the complete earlywood zone when compressed in the radial direction is shown in Fig. 21b. In the diagrams the strain is being defined as nominal strain, i.e. as the change in length per initial length.

6.4. Nonlinear fracture model

The nonlinear fracture mechanics model employed in this study corresponds to a fictitious crack model (FCM) [6,23]. The model is easily implemented by introducing special crack elements. The fracture of the material is modelled by introducing two fictitious crack surfaces. The distance between these surfaces is initially zero. By introducing stresses and relative displacements between the surfaces, the fracturing process can be modelled in a simple and well-defined way.

In the following, the tensile stress and the relative displacement normal to the fracture zone are denoted as σ_n and δ_n, respectively, and the shear stress and

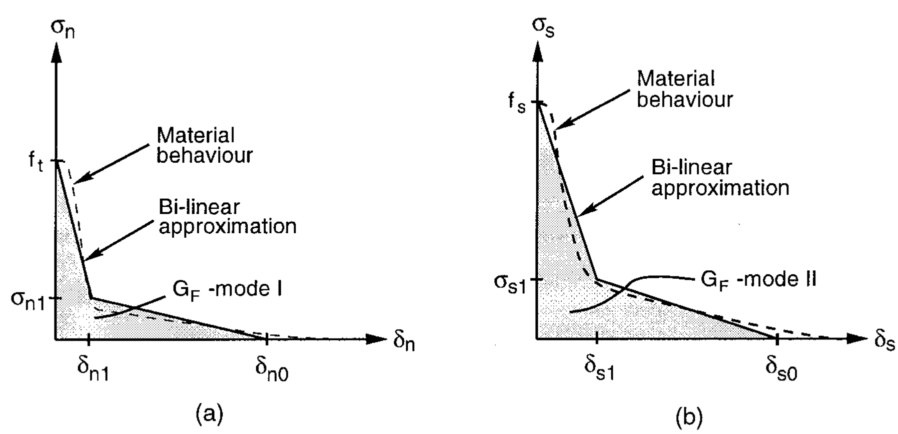

Fig. 22. Approximation of fracturing properties using bilinear stress-displacement relations. (a) Pure opening mode. (b) Pure shearing mode.

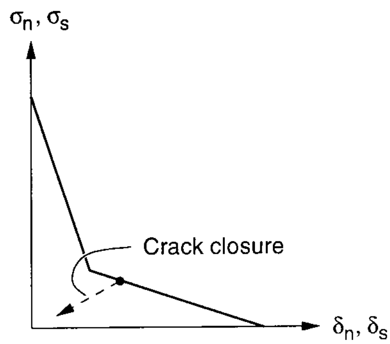

Fig. 23. Illustration of crack closure.

relative shear displacement as σ_s and δ_s. The fracturing properties of the pure opening mode (mode I) and the pure shearing mode (mode II) expressed as softening stress-relative displacement relations, are approximated using bilinear curves based on experimental results [6], as shown in Fig. 22. The tensile and shear strengths are denoted as f_t and f_s, respectively. The displacements for which the stresses are zero, representing a complete fracture, are denoted as δ_{n0} and δ_{s0}, the corresponding breakpoints on the curves being designated as σ_{n1} and δ_{n1} and as σ_{s1} and δ_{s1}, respectively.

To model a mixed mode fracture, the coupling between the softening properties in tension and shearing must be considered. The stress components σ_n and σ_s are here simply expressed as functions of the relative displacements δ_n and δ_s according to

$$\sigma_n = \sigma_n(\delta_n,\delta_s) = \sigma_n(\delta_n)\left(1 - \frac{\delta_s}{\delta_{s0}}\right)^m$$

$$\sigma_s = \sigma_s(\delta_n,\delta_s) = \sigma_s(\delta_s)\left(1 - \frac{\delta_n}{\delta_{n0}}\right)^n \tag{32}$$

where $\sigma_n(\delta_n)$ and $\sigma_s(\delta_s)$ denote the material description for the pure opening and the pure shearing mode, respectively, and where m and n are mixed-mode coupling parameters. For $m=n=0$ there is no coupling between the tensile and the shearing behaviour. Suitable values for m and n are in the range of 1–10. In this study a value of 5 has been chosen for both m and n.

For the case of compression perpendicular to the crack plane, a Coulomb friction model is used. This means that the shearing capacity is increased according to

$$\sigma_s = \sigma_s(\delta_s)\left(1 - \frac{\delta_n}{\delta_{n0}}\right)^n + \sigma_p\mu \tag{33}$$

where σ_p is the contact pressure at the fracture zone and μ is the coefficient of friction.

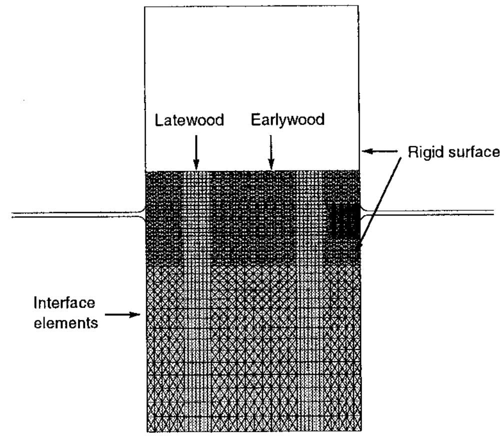

Fig. 24. Example of finite element models used in the simulations.

If the crack width does not increase monotonically, crack closure may occur. For the applications in mind here, involving complex loading conditions and deformation patterns, crack closure can take place and must therefore be taken into account. In the present model, it has been assumed that the crack closing path reverts to the origin, implying that the entire crack width that developed is recoverable, as illustrated in Fig. 23.

7. Numerical examples—Initial defibration of wood

In this section some of the large number of numerical simulations on the initial defibration of wood that were performed will be presented and be compared with experimental results. The basis for the simulations was an experimental investigation, some of the results of which are shown in Fig. 4.

In the finite element analysis, the problem was analysed as constituting a two-dimensional static problem under plane strain conditions using an implicit integration scheme. The elements employed were four-noded bilinear quadrilateral elements for the latewood zones and three-noded linear triangular elements for the earlywood. The tests indicated large deformations to occur in the earlywood which was simulated by a rate formulation based on the Jauman stress rate and a logarithmic strain rate [17]. Triangular elements were thus used for the earlywood zones since such elements are relatively insensitive to large distortions. Crack elements were introduced between the solid elements at locations where large tensile and/or large shearing stresses occurred. When the strength of the material was reached, these elements captured the softening behaviour of the material.

The steel that bounded the wood specimen was modelled as rigid surfaces. Interface elements were used to describe the contact forces between these rigid surfaces and the wood. A Coulomb friction model was employed, the coefficient of friction between the steel and the specimen being set to 0.25. The fit of the specimens between the steel plates was assumed to be perfect, a somewhat crude assumption if accurate description of the contact forces is to be expected. The gap between the steel grips was set to 0.1 mm, just as in the experiments. Fig. 24 shows a typical finite element mesh used in the simulations.

In the following, various results of the numerical simulations are presented and are compared with experimental results. Two different specimen types are described, the wood in the one being subjected to a shear loading in the radial direction and in the other to shear loading in the tangential direction. The deformation and fracture processes predicted by the simulations agree well with the experimental results, both in the case of the dry and of the wet specimens. This can be seen in Fig. 25 in which the simulated deformation and fracture processes for various test series are compared with the actual experimental processes for typical specimens in these test series.

The location of the fracture zones predicted by the FE-simulations and the large deformations within the earlywood appear to have been captured very well by the modelling employed. Comparing the force–displacement relations in the horizontal direction obtained in the simulations with the corresponding experimental curves indicates the agreement in terms of the shape of the curves to be relatively good. The overall stiffness in the simulations is in general somewhat too high, however, and for the case considered in Fig. 25b the maximum load is reached at a lower shearing displacement than in the experiments. These differences can partly be explained by its being assumed in the simulations that there is a perfect fit of the specimen between the steel plates. In most of the experiments there were certain small gaps between the specimen and the steel plates present, due to difficulties in preparing specimens of exactly correct dimensions. In addition, the stiffness may have been overestimated through use of a somewhat too coarse finite element mesh consisting of triangular elements.

Due to the large deformations, the complex behaviour of the material and the contact conditions present, numerical difficulties might arise when simulations of this character are performed. It was thus not possible in all cases to fully predict the behaviour of the specimens during the complete course of loading. However, the major characteristics of the deformation and fracture processes that occurred could be surprisingly well predicted, consisting uncertainties in about selecting proper material parameters.

8. Concluding remarks

In the present paper, both experimental and numerical work concerning the mechanical properties of cellular materials such as wood have been presented. The experimental work involved both experiments at the microstructural level and the testing of wood specimens. Models of the microfibrils in the cell wall as well as of the cellular structure of wood were developed with the aim of determining the stiffness and shrinkage properties of wood. Numerical studies were also carried out.

Models for determining the mechanical properties of wood based on its microstructure were proposed. The models concern the chain of properties extending from the mechanical properties of the various chemical constituents of the cell wall to the average mechanical properties of a growth ring. Models of the microfibril were created with the aim of determining the properties of the various cell-wall layers. These models are based on the geometry of the microfibril and the properties of its constituents.

The experimental and modelling work in this study can be extended in various ways. The present investigation on homogenization focussed on the linear stiffness and shrinkage properties. There are many other important properties of wood, related to its plasticity, fracturing, mechanosorption and other types of nonlinear material behaviour for which homogenization theory can be applied. Further development of the models should involve studies of these aspects of behaviour as well. Better knowledge of the geometry and the mechanical properties of wood at both the microstructural level and the growth-ring level may be needed in order to develop the present models further for determining stiffness and shrinkage properties. To improve these models, better knowledge of the mechanical properties of the chemical constituents in the microfibril should likewise be gained. Since the microfibril angles in the various layers of the cell walls differ and they may differ in the radially and tangentially oriented cell walls, experimental determination of these angles is necessary to improve the models. In the present model, the cells are assumed to be infinitely long in the longitudinal direction. A possible extension of the models would be to include the end-caps of the cells in the model. The degree of variation in the shapes of the cells and in the density within the growth ring are factors that are important to take into account in modelling larger cell structures. In the growth-ring model based on the cells being hexagonal, the cells are assumed to be equal in width in the radial direction. A more correct distribution of the widths of the cells in this direction would provide more accurate results. It would be of clear interest in the long run to determine a more complete chain from the microstructural

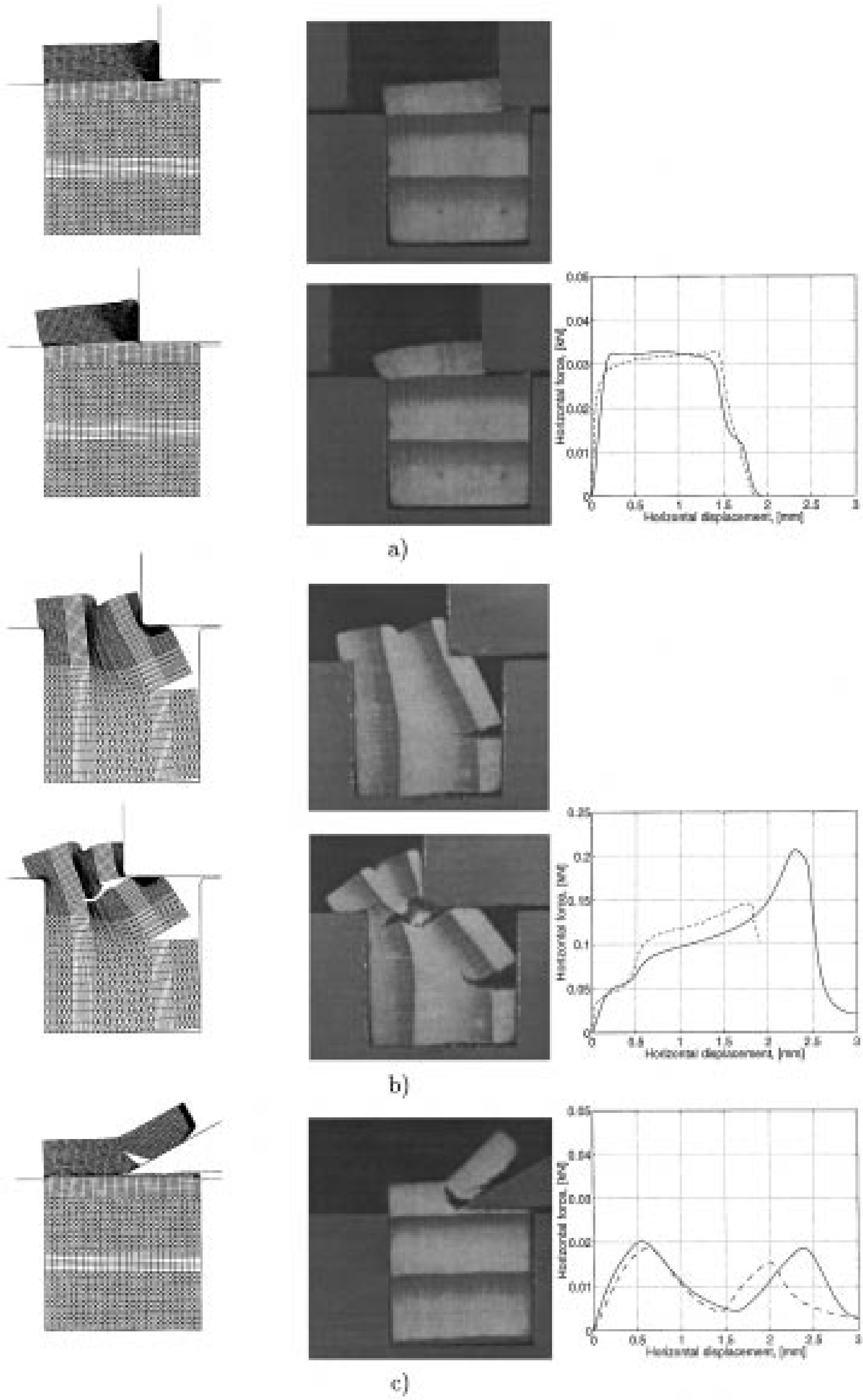

Fig. 25. Comparison between numerical simulation and experimental results. The solid curve depicts the experimental result and the dashed curve the numerical result. (a) Loading in the tangential direction. (b) Loading in the radial direction. (c) Knife loading in the tangential direction.

properties to the properties of boards and planks. Such models must also include such imperfections as knots and fibre deviations. The present study is seen to represent a valuable step forward in the direction of a more complete micro–macro modelling approach for wood.

Another aim of this study was to obtain certain fundamental insight into the mechanics of the initial defibration process. Simulations were performed in order to discover material models appropriate for the complex material behaviour observed in the experiments, as well as to identify problems that can arise when numerical simulations of this sort are performed. It can be concluded that good agreement between the simulations and the experiments was obtained using the material modelling that was adopted. However, when simulations of this kind are performed, numerical difficulties may arise due to the deformations being very large, to local material instabilities or to contact conditions. Material modelling is a key matter in performing defibration simulations. The experiments indicate the importance of taking account of differences between earlywood and latewood. Unfortunately, little experimental work has been carried out to determine the mechanical properties of these two wood types separately. Due to the lack of experimental data, some of the properties adopted could not be verified experimentally. Further experimental work is needed in order to determine the elastic, plastic and fracture mechanical properties of earlywood and latewood separately.

References

[1] Petersson H. Fracture design criteria for wood in tension and shear. In: Pacific Timber Engineering Conference, Gold Coast Australia, 11–15 July, 1994.
[2] Petersson H. Fracture mechanics—an integral view from micro to macro structure. In: Proceedings of the 1996 International Conference on Wood Mechanics, Stuttgart, 1994. p. 511–28.
[3] Dahlblom O, Ormarsson S, Petersson H. Simulation of wood deformation processes in drying and other types of environmental loading. Ann Sci For 1996;53:857–66.
[4] Petersson H, Dahlblom O, Ormarsson S, Persson K. Moisture distortion modelling of wood and structural timber. In: Mechanical Performance of Wood and Wood Products, Copenhagen, 16–17 June, 1997 COST action E8.
[5] Ormarsson S. A finite element study of the shape stability of sawn timber subjected to moisture variations. Report TVSM-3017, Lund University, Sweden, 1995.
[6] Holmberg S. Deformation and fracture of wood in initial defibration process. Report TVSM-3019, Lund University, Sweden, 1997.
[7] Kollman KFP, Côte WA. Principles of wood science and technology, 1. Solid wood. Berlin: Springer, 1968.
[8] Bodig J, Jayne BA. Mechanics of wood and wood composites. New York: Van Nostrand Reinhold, 1982.
[9] Barett JD. Fracture mechanics and the design of wood structures. In: A Royal discussion in fracture mechanics in design and service. London, 1981. p. 217–26.
[10] Persson K. Modelling of wood properties by a micromechanical approach. Report TVSM-3020, Lund University, Sweden, 1997.
[11] Gibson LJ, Ashby MF. Cellular solids. Structure and properties. Oxford: Pergamon, 1988.
[12] Stefansson F. Mechanical properties of wood at microstructural level. Report TVSM-5057, Lund University, Sweden, 1994.
[13] Price AT. A mathematical discussion on the structure of wood in relation to its elastic properties. Phil Trans R Soc, Lond 1928;228:1–62.
[14] Koponen S, Toratti T, Kanerva P. Modelling longitudinal elastic and shrinkage properties of wood. Wood Sci Technol 1989;23:55–63.
[15] Kahle E, Woodhouse J. The influence of cell geometry on the elastic constants of softwood. J Mater Sci 1994;29:1250–9.
[16] Persson K, Petersson H, Stefansson F. Mechanical properties of wood cell structures. In: Plant Biomechanics, Reading, UK, 7–12 September, 1997.
[17] Hibbitt, Karlsson & Sorensson Inc. ABAQUS Theory manual, Version 5.4, Pawtucket, RI, 1994.
[18] Bensoussan A, Lions JL, Papanicolaou G. Asymptotic analysis for periodic structures. Amsterdam: North-Holland, 1978.
[19] Carrington H. The elastic constants of spruce. Phil Mag 1923;45:1055–7.
[20] Hearmon RFS. The elasticity of wood and plywood. In: Forest Products Research Special Report, Vol. 7. London: HMSO, 1948.
[21] deSouza Neto EA, Perić D, Owen DRJ. Finite strain implementation of an elastoplastic model for crushable foam. In: Wiberg N-E, editor. Advances in finite element technology. Barcelona: CIMNE, 1995.
[22] Schreyer HL, Zuo QH, Maji AK. Anisotropic plasticity model for foams and honeycombs. J Engng Mech 1994;120:1913–30.
[23] Hillerborg A, Modeer M, Petersson PE. Analysis of crack formation and crack growth in concrete by means of fracture mechanics and finite elements. Cement Concrete Res 1976;6:773–82.